Including Special Secion:
Silicate Melts and Mantle Petrogenesis (in Memory of Christopher M. Scarfe)

Journal of Geophysical Research

Non-Newtonian Rheology of Igneous Melts at High Stresses and Strain Rates: Experimental Results for Rhyolite, Andesite, Basalt, and Nephelinite

SHARON L. WEBB AND DONALD B. DINGWELL

Bayerisches Geoinstitut, Universität Bayreuth, Bayreuth, Federal Republic of Germany

The stress-strain rate relationships of four silicate melt compositions (high-silica rhyolite, andesite, tholeiitic basalt, and nephelinite) have been studied using the fiber elongation method. Measurements were conducted in a stress range of 10–400 MPa and a strain rate range of 10^{-6} to 10^{-3} s^{-1}. The stress-strain rate relationships for all the melts exhibit Newtonian behavior at low strain rates, but non-Newtonian (nonlinear stress-strain rate) behavior at higher strain rates, with strain rate increasing faster than the applied stress. The decrease in calculated shear viscosity with increasing strain rate precedes brittle failure of the fiber as the applied stress approaches the tensile strength of the melt. The decrease in viscosity observed at the high strain rates of the present study ranges from 0.25 to 2.54 $\log_{10}$ Pa s. The shear relaxation times τ of these melts have been estimated from the low strain rate, Newtonian, shear viscosity, using the Maxwell relationship $\tau = \eta_s/G_\infty$. Non-Newtonian shear viscosity is observed at strain rates ($\dot{\varepsilon} = $ time^{-1}) equivalent to time scales that lie 3 $\log_{10}$ units of time above the calculated relaxation time. Brittle failure of the fibers occurs 2 $\log_{10}$ units of time above the relaxation time. This study illustrates that the occurrence of non-Newtonian viscous flow in geological melts can be predicted to within a $\log_{10}$ unit of strain rate. High-silica rhyolite melts involved in ash flow eruptions are expected to undergo a non-Newtonian phase of deformation immediately prior to brittle failure.

1. INTRODUCTION

The rheology of magmas is a critical factor in determining the mode of occurrence of igneous rocks [*Harris et al.*, 1970]. A complete understanding of magma rheology requires a comprehensive description of the rheology of the melt phase [*Shaw*, 1965]. Most studies of shear viscosities of silicate melts have been conducted at conditions of relatively high temperatures and low viscosities (see compilations by *Bottinga and Weill* [1972], *Bansal and Doremus* [1986], and *Ryan and Blevins* [1987]). In cases where the stress-strain rate relationship has been investigated over a significant range of strain rate, both Newtonian behavior (i.e., linear stress-strain rate relationship) [e.g., *Scarfe et al.*, 1983] and non-Newtonian behavior [e.g., *Li and Uhlmann*, 1970; *Simmons et al.*, 1982; *Spera et al.*, 1982] have been observed.

Dingwell and Webb [1989] suggested that the strain rates above which non-Newtonian behavior is expected to occur in silicate melts can be predicted from linear viscoelastic theory. The relaxation (equilibration) time of a melt in response to an applied shear stress is given by the Maxwell relation:

$$\tau = \eta_s/G_\infty \qquad (1)$$

where τ is the relaxation time, η_s is the zero frequency Newtonian shear viscosity, and G_∞ is the infinite frequency elastic shear modulus of the melt. Given the relative invariance of the value of G_∞ in liquids in general and silicate melts in particular (for further discussion, see *Angell and Torrell* [1983] and *Dingwell and Webb* [1989]), the relaxation time τ (and relaxation strain rate $\dot{\gamma} = \tau^{-1}$) is proportional to the relaxed (Newtonian) shear viscosity of the melt. The Maxwell relationship applies for a single relaxation time. Most silicate melts require a distribution of relaxation times centered on an average relaxation time. It has been shown [*Mills*, 1974; *Sato and Manghnani*, 1985; *Rivers and Carmichael*, 1987] that the Maxwell relationship provides a good approximation of the average relaxation time of silicate melts. The present study was conducted to investigate the occurrence of non-Newtonian rheology in geologic melts, and to test the applicability of the Maxwell relation.

The fiber elongation technique is one of the viscometry methods that permits the determination of viscosity at much lower temperatures, higher viscosities (10^9 to 10^{15} Pa s), and higher stresses ($10^{8.6}$ Pa) than are possible with the concentric cylinder method (10^5 Pa s and 10^6 Pa). This technique was chosen for the present study as the accessible strain rates are within an order of magnitude of the calculated relaxation strain rates of the melt.

2. EXPERIMENTAL METHOD

Four melt compositions, chosen to represent a wide chemical range of geological melts, were investigated. The compositions are a high silica rhyolite from Little Glass Mountain (LGM), an andesite from Crater Lake, a tholeiitic basalt from Hawaii, and an "average" nephelinite from the compilation by *Chayes* [1975] [see *Mysen*, 1987]. The melt compositions are presented in Table 1.

The rhyolite starting material was an obsidian collected from Little Glass Mountain, California (by M. Carroll). A cobble of the obsidian was broken into chips a few centimeters in size. Approximately 100 g of these chips were melted stepwise into a 50 cm^3 thin-walled Pt$_{95}$Au$_5$ crucible in a MoSi$_2$ element box furnace and held at 1675°C overnight. The melted obsidian (hereafter referred to as rhyolite) was removed from the box furnace and loaded into a second MoSi$_2$ box furnace equipped with a concentric cylinder viscometer [*Dingwell*, 1989]. The viscometer Pt$_{80}$Rh$_{20}$ spindle was used to stir the rhyolite melt at 1650°C for 8 days. The melt was periodically inspected for bubble content by observation of the rhyolite wetting the spindle. Fibers ap-

TABLE 1. Melt Compositions

	LGM	CLA	HTB	NEP
SiO_2	77.7	62.04	51.20	39.95
TiO_2	0.06	0.76	2.59	2.76
Al_2O_3	13.0	16.77	13.54	13.50
$Fe_2O_3^*$	—	3.29	9.44	10.84
FeO*	0.71	1.98	2.36	0.95
MnO	0.03	0.25	0.17	0.28
MgO	0.05	3.25	7.30	7.86
CaO	0.53	5.07	10.50	12.94
Na_2O	4.06	5.01	2.48	4.54
K_2O	4.18	1.72	0.50	3.32

LGM analysis, average of nine, Camebax microprobe 15 kV, 10 nA on brass, 15 s count times. In weight percent.
*Fe_2O_3/FeO ratio by ^{57}Fe Mössbauer spectroscopy.

proximately 30 cm long were drawn from the rhyolite melt by retracting the spindle from the furnace. These fibers were examined using optical microscopy and X ray diffractometry. They were found to be both crystal- and bubble-free. The glass fibers were broken to shorter lengths (with diameters ranging from 0.1 to 0.6 mm) and the ends of the fibers were fired in the flame of an oxy-acetylene torch to produce beads approximately 1.5 mm in diameter. The lengths of the beaded fibers varied from 10 to 18 mm. The starting materials for the andesite, basalt, and nephelinite melts were 10 g oxide plus carbonate powder mixes which were directly fused in $Pt_{95}Au_5$ crucibles, at 1500°C for 10 hours with occasional hand stirring using an alumina rod. After removal of the crucible from the furnace, 1-m-long fibers were drawn from these melts using the alumina rod. These fibers were further processed in the same manner as the rhyolite fibers.

The fiber strain was measured using a commercial dilatometer (Model TMA 402, Netzsch Gerätebau, Selb, West Germany). This instrument is a vertically mounted silica glass dilatometer equipped with a Kanthal wire-wound three-zone furnace. Each furnace zone is controlled independently by an electronic set-point controller resulting in a furnace hot zone (±1°C) of 5 cm. The temperature is measured by a type S ($Pt-Pt_{90}Rh_{10}$) thermocouple suspended approximately 3 mm radially distant from the fiber. A 1°C correction was applied to the measured temperature due to a radial temperature gradient. The silica glass holder of the dilatometer supports the beaded glass fiber in a fork. A second silica glass rod holds the lower bead of the fiber in tension. This second rod is connected to a weight pan at the top of the dilatometer via a vanadium rod. Tensile stress is applied to the sample by loading weights on the weight pan.

The elongation of the fiber is monitored by the movement of the vanadium rod through the center of a calibrated linear voltage displacement transducer (LVDT). The lower silica rod has a ~17 mm travel. The maximum travel determined by the LVDT is, however, 2.5 mm. Therefore, in order to obtain total strains greater than 10^{-1} (extension of the fiber from the original ~15 mm to a total of ~30 mm) it was necessary to rezero the LVDT during the experiment. The need to rezero the LVDT, together with the limited amount of travel available, limits the accessible strain rate range to 10^{-7} to 10^{-4} s^{-1}. A shear viscosity of 10^{12} Pa s was found to be optimal for the attempt to achieve non-Newtonian viscosities. The much higher viscosity and much larger cross-sectional area of the silica glass support rod ensure

that insignificant relaxation of the silica occurs during the experiments.

In the present determinations of viscosity, a tensile stress is applied to a melt fiber and the viscosity is determined as the ratio of the applied stress to the observed strain rate. In this geometry, the observed viscosity η_{elong} is the elongational viscosity and is related to the shear viscosity η_s by

$$\eta_{elong} = \frac{\sigma}{\dot{\varepsilon}} = \frac{9\eta_v\eta_s}{3\eta_v + \eta_s} \qquad (2)$$

where η_v is the volume viscosity [e.g., Herzfeld and Litovitz, 1959; Ferry, 1980; Mazurin, 1986].

Each fiber was initially annealed at temperature with a load of ~10 MPa for a period of 10^4 s (strain ≈ 5×10^{-2}). This equilibration time is 2 orders of magnitude greater than both the shear and volume relaxation times of a melt with $\eta_v = \eta_s \approx 10^{12}$ Pa s and G_∞ (shear modulus) ≈K_∞ (bulk modulus) ≈25 GPa ($\tau_v = \tau_s = 40$ s). The determinations of non-Newtonian viscosity were begun with this initial stress of 10 MPa ($\dot{\varepsilon} \sim 10^{-5}$; $\eta_{elong} \sim 10^{12}$ Pa s); the applied stress being increased in steps of ~25% until either the fiber broke or the end of travel of the lower silica rod was reached. After the application of each additional mass, the elongation of the fiber was monitored on a 1.2-s time interval for 300 s. The applied stress and resultant strain rate were recalculated at each 1.2-s interval in order to allow for the changes in the dimensions of the fiber. Equation (2) is derived using linear viscoelastic theory. This linear theory applies for the case where $\dot{\varepsilon}\tau < 1$ [Christensen, 1982]. In the present study, where $\tau \sim 40$ s, strain rates less than 2.5×10^{-2} s^{-1} are within the regime of the applicability of linear viscoelastic theory. This range of strain rates encompasses all of the data presented here.

For strain rates of the order 10^{-6} s^{-1}, errors in calculated viscosity were approximately 0.1 $\log_{10}$ Pa s; with increasing strain rate to 10^{-4} s^{-1} this error was reduced to 0.01 $\log_{10}$ Pa s. It was found that constant values of strain rate (within the 5–25% uncertainty associated with the calculated strain rate for strain rates <5×10^{-5} s^{-1}) were obtained within 100 s of applying the weight. For a melt with $\tau = 40$ s, the calculated unrelaxed strain rate is within 8% of the relaxed strain rate for times greater than 100 s, indicating that the stress-strain rate behavior approaches equilibrium within the time scale of the measurement and that the calculated viscosities are within error of the relaxed viscosities of the melt. This analysis neglects any changes in cross-sectional area and length due to elastic deformation. For the strains (>5 × 10^{-3}) involved in the present experiments, the effect of elastic deformation on the calculated stress and strain rate is negligible (<0.02%). The quoted uncertainties in viscosity include the errors in length and cross-sectional area of the fibers (the maximum taper of the fibers used was 7%; increasing the error in viscosity by 0.01 $\log_{10}$ units), the errors in strain rate determination and a further 0.05 $\log_{10}$ Pa s error due to temperature fluctuations and gradients.

Although infinite shear strains are possible in a melt, volume strain must be limited in magnitude [Mazurin, 1986]. The volume viscosity of a melt therefore approaches an infinite value with increasing time, and (2) becomes

$$\eta_{elong} = 3\eta_s \qquad (3)$$

[Ferry, 1980; Mazurin, 1986] for time ≫τ. The viscosities quoted here are the shear viscosities of the melts. For
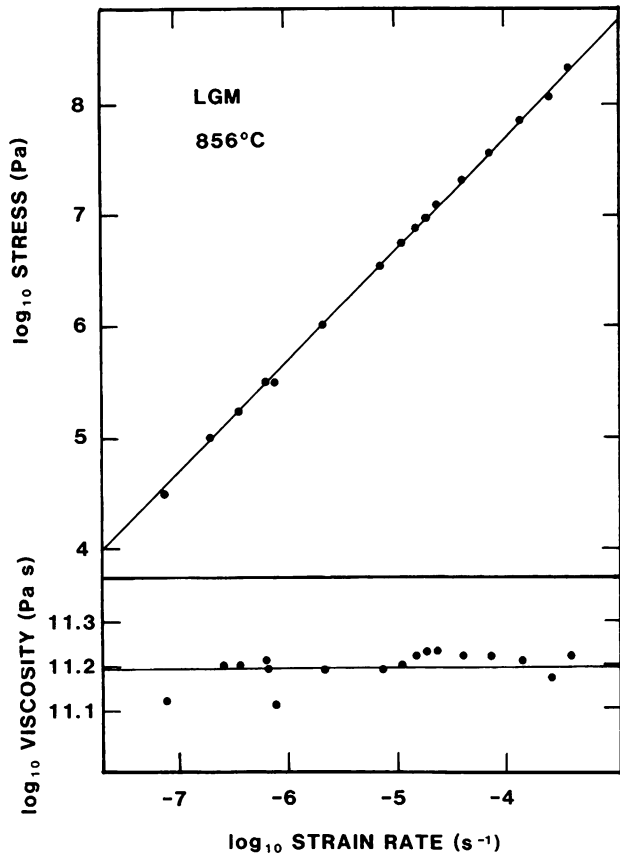
Fig. 1. Stress and shear viscosity versus strain rate for Little Glass Mountain rhyolite at 856 ± 1°C. The errors in viscosity are ±0.05 $\log_{10}$ Pa s.

Fig. 2. Shear viscosity of Little Glass Mountain rhyolite as a function of reciprocal temperature. The hollow data points are not relaxed and are not included in the fit to the data.

periods >100 s, the shear viscosity calculated using (3) is at most 0.02 $\log_{10}$ Pa s less than the relaxed shear viscosity.

Due to the limited strain available, it was not possible to use the extension of the fiber, and accompanying decrease in cross-sectional area, to increase the stress resulting from the application of one weight from the Newtonian to the non-Newtonian stress-strain rate regime. In a preliminary study of the viscosity of Little Glass Mountain rhyolite at $T = 856°C$, Newtonian shear viscosity was observed over a stress range of 30 kPa to 200 MPa and a strain rate range of 8×10^{-8} to 4×10^{-4} s^{-1}. Having observed Newtonian viscosity over this large range of stress and strain rate, the stress employed in the measurements was increased in order to produce strain rates approaching the calculated relaxation strain rate of the melts.

3. RESULTS AND DISCUSSION

The viscosity of LGM rhyolite determined over four orders of magnitude of strain rate ($10^{-7.5}$ to $10^{-3.5}$ s^{-1}) is illustrated in Figure 1. A Newtonian shear viscosity of 11.19 ± 0.10 $\log_{10}$ Pa s was observed in this range of strain rates. The viscosity of LGM rhyolite was further measured over a temperature range of 650°–1000°C at smaller strain rates. The relaxed (Newtonian) viscosity is illustrated in Figure 2. The shear viscosities are an Arrhenian function of temperature with an activation energy of 440 kJ mol^{-1}.

The critical experiments illustrating non-Newtonian behavior are illustrated in Figures 3 and 4. The viscosity of

NBS 710 soda lime silicate melt at 565° ± 1°C is plotted in Figure 3 as a function of strain rate. The shear viscosity is 11.77 ± 0.07 $\log_{10}$ Pa s in the low strain rate range of 1–4 × 10^{-5} s^{-1}. At strain rates above 4×10^{-5} s^{-1} the viscosity decreases to a value of 9.23 $\log_{10}$ Pa s before the fiber
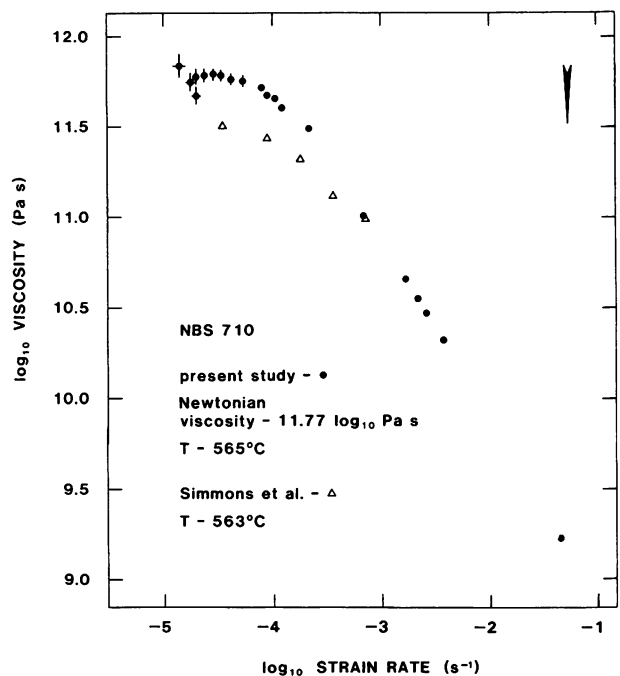
Fig. 3. Shear viscosity of NBS 710 soda lime silicate as a function of strain rate. The arrow indicates the calculated relaxation strain rate for a Newtonian viscosity $10^{11.77}$ Pa s.
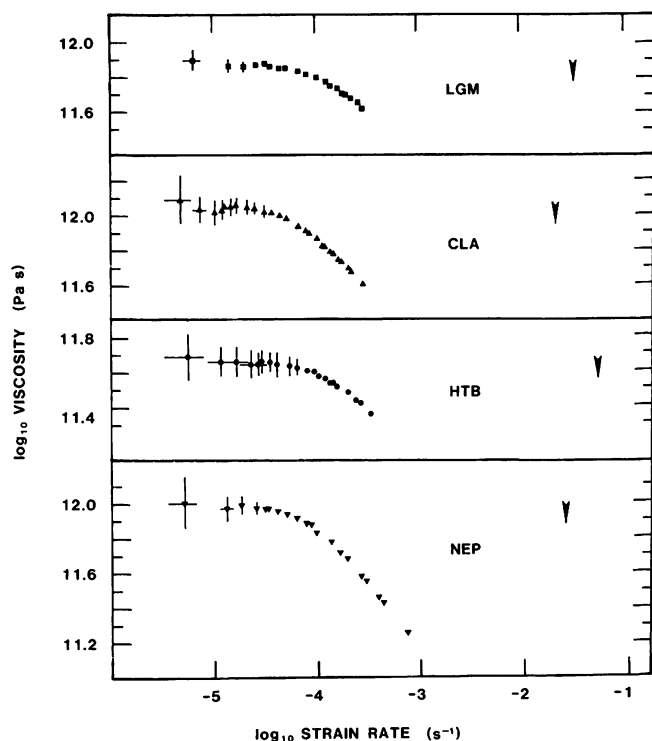
Fig. 4. Shear viscosity of Little Glass Mountain rhyolite, Crater Lake andesite, Hawaiian tholeiite, and nephelinite as functions of strain rate. The arrows indicate the calculated relaxation strain rates.

breaks. This behavior confirms the results of *Simmons et al.* [1982] which are plotted in Figure 3 for comparison.

In Figure 4, high strain rate viscosity data for the rhyolite (LGM), andesite (CLA), basalt (HTB), and nephelinite (NEP) are plotted as functions of strain rate, at temperatures of $818 \pm 1°C$, $754 \pm 1°C$, $716.5 \pm 1°C$, and $673.5 \pm 1°C$, respectively. Each melt exhibits qualitatively similar behavior, with viscosity remaining constant over a range of low strain rates and decreasing as the strain rate is increased. The $\log_{10}$ stress versus $\log_{10}$ strain rate for these melts is plotted in Figure 5. The departure from Newtonian behavior is illustrated by the departure from a slope of 1 at strain rates $>5 \times 10^{-5}$ s^{-1}.

At this point, it is necessary to consider the possible effects of viscous heating of these fibers, as the observed decrease in viscosity could be caused by increasing temperature. Taking the two extremes of viscosity decrease (LGM and NBS 710), the temperature increases required to reduce the viscosity by 0.25 and 2.54 $\log_{10}$ Pa s are 13°C and 63°C, respectively. The rate of doing work on the fiber can be calculated from

$$dW/dt = \sigma \dot{\varepsilon} V \qquad (4)$$

[*Nye*, 1957], where V is the volume of the fiber. For the rhyolite and NBS fibers, the rate of doing work is 1.5×10^{-5} and 1.0×10^{-5} J s^{-1}, respectively. Following the analysis of *Simmons et al.* [1982], the lower limit to the rate of heat loss by the fiber can be calculated from the radiative heat transfer coefficient H:

$$H = 4eST^3 \qquad (5)$$

where e is the emissivity, S is the Stefan-Boltzmann constant $(5.67 \times 10^{-8}$ J s^{-1} m^{-1} K$^{-4})$, and T is absolute temperature. Assuming an emissivity of 0.3, H(LGM) $= 88$ J K^{-1} m^{-2} s^{-1} and H(NBS) $= 40$ J K^{-1} m^{-2} s^{-1}. The rate of heat loss by radiative transfer is

$$dQ/dt = HA\Delta T \qquad (6)$$

where A is the surface area of the fiber and ΔT is the temperature difference between the furnace and fiber. Setting (4) = (6), the maximum temperature increase in the fiber (above that of the furnace) is 0.01°C and 0.15°C for the rhyolite and the NBS melts, respectively. Increasing the assumed value of emissivity further reduces the calculated temperature difference. These calculated maximum increases in temperature due to viscous heating are much smaller than the temperature increase required to reduce the shear viscosities of these melts by the observed amounts.

Relaxation Curve

The temperature at which each melt composition was investigated was chosen in order to set the shear viscosity to $\sim10^{12}$ Pa s. The relaxation time of such melts is calculated from (1) to be 40 s, corresponding to a relaxation strain rate of $\sim2.5 \times 10^{-2}$ s^{-1}. The calculated relaxation strain rates $(\dot{\gamma})$ are plotted, for each composition, as arrows in Figures 3 and 4. The deviation from a Newtonian stress-strain relationship occurs at strain rates which are ~3 orders of magnitude less than the calculated relaxation strain rates. In the case of melts described by a single relaxation time, a 2% deviation from relaxed (equilibrium) behavior is expected to occur 2 orders of magnitude below the relaxation strain rate. A number of studies of silicate melts in the glass transition region (e.g., torsional [*Mills*, 1974] and ultrasonics [*Sato and Manghnani*, 1985]), however, indicate more complex relaxation behavior than that described by a single relaxation time. Any distribution of shear relaxation times will result in a broadening of the width of the relaxation zone and the occurrence of nonrelaxed behavior at lower strain rates than predicted from single relaxation strain rate theory.

Microscopic Considerations

Recent ^{29}Si NMR studies of relaxation in silicate melts ($Na_2Si_2O_5$ [*Liu et al.*, 1988] and $K_2Si_4O_9$ [*Stebbins*, 1988]) have resulted in the determination of timescales for the exchange of Si-O bonds. This time scale corresponds to the macroscopic structural relaxation time scale obtained from the Maxwell relation. Thus it appears that the glass transition results from the exchange of Si-O bonds. This implies that above the glass transition (i.e., at longer time scales or higher temperatures), in relaxed silicate melts, no individual extended species, defined by Si-O bonds (e.g., Si-O-Si-based polymers) can exist on the time scale of observation.

The success of the Eyring equation [*Shimizu and Kushiro*, 1984] in relating viscosity to oxygen diffusion implies that both oxygen diffusion and viscous flow proceed by the translation of single oxygen anions. The onset of non-Newtonian shear viscosity can be viewed as a consequence of the rate of applied shear deformation approaching the equilibrium rate of Si-O bond exchange. This interpretation is supported by the agreement of the observed exchange
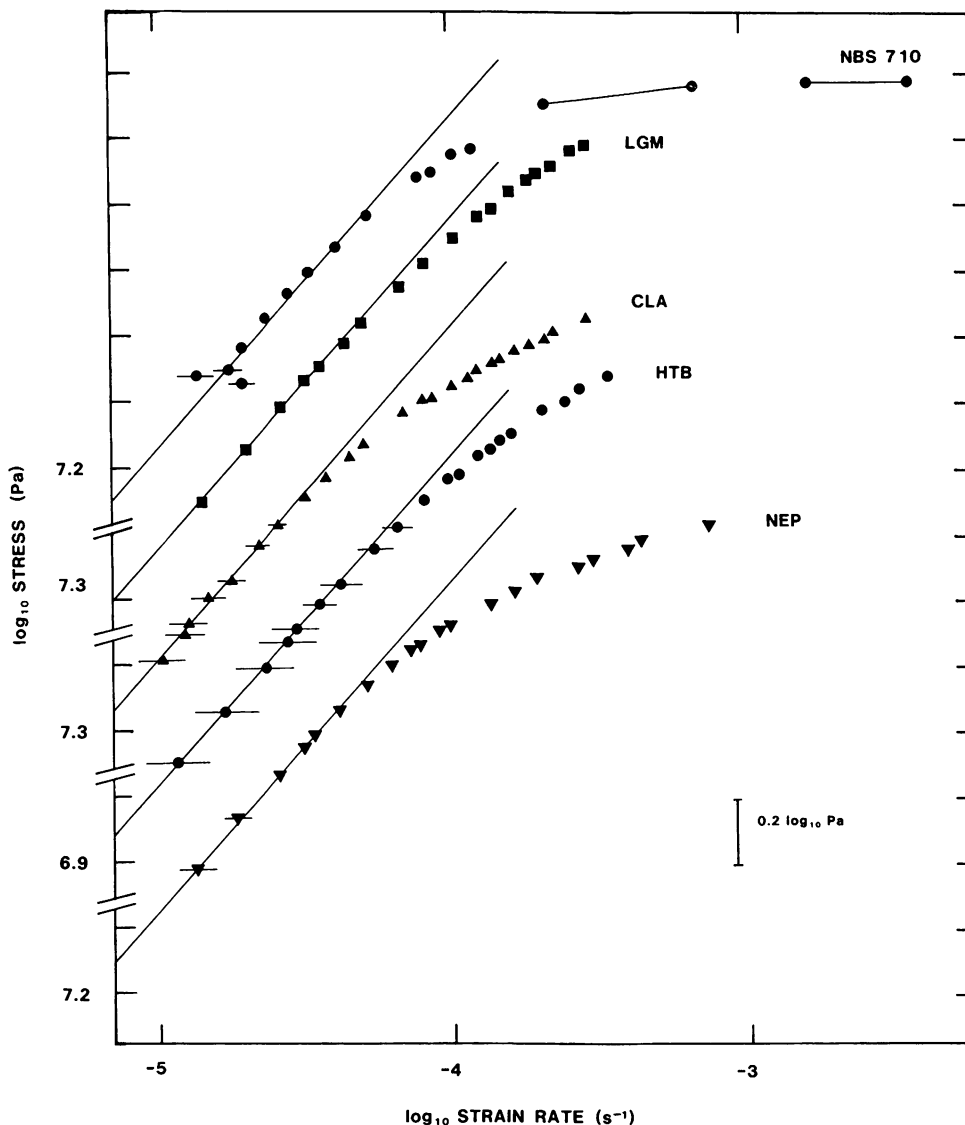
Fig. 5. Stress versus strain rate for NBS 710 soda lima silicate, Little Glass Mountain rhyolite, Crater Lake andesite, Hawaiian tholeiite, and nephelinite. Lines of slope = 1, (representing a linear stress-strain rate relationship) are fit to each set of data.

frequency of Si–O bonds, the macroscopic structural relaxation frequency $(2\pi\tau)^{-1}$ and the calculated jump frequency of diffusing oxygen anions ($Dx^{-2} = 2\pi f_{jump}$) [Dingwell and Webb, 1989].

Strain

The present study underlines an important distinction to be made between low strain measurements of the glass transition (i.e., frequency domain studies such as mechanical torsion or ultrasonic wave propagation experiments) and high strain measurements such as fiber elongation. Both types of experiments observe non-Newtonian viscosity as a frequency or strain rate dependence of the stress-strain rate ratio. In frequency domain experiments, the frequency of the applied stress may be increased through the glass transition frequency $(\tau^{-1} = 2\pi f)$ and the shape of the relaxation function recorded. In time domain experiments, however, the stress required to reach strain rates approaching the relaxation strain rate $\dot\gamma$ approximates the tensile strength of

the melt, and the material fails before $\dot\gamma$ is reached. Figure 6 is a plot of the strain rate-temperature location of the propagation of longitudinal shock [Rigden et al., 1988] and ultrasonic [Sato and Manghnani, 1985] waves in rhyolitic melts. The relaxation or τ curve of the LGM rhyolite is plotted using the present viscosity data of Figure 2 at lower temperatures and the method of Shaw [1972] at high temperatures in combination with the Maxwell relation.

The strain rate-temperature range of two time domain methods that have been used with rhyolite melts are also plotted in Figure 6; the concentric cylinder [Dingwell et al., 1985; Spera et al., 1988] and fiber elongation (this study) methods. The present study illustrates that, as in frequency domain experiments, the fiber elongation technique records the onset of non-Newtonian behavior in the melt. It is expected, however, that the large nonequilibrium strains associated with this technique will result in structural anisotropy of the melt [Brückner, 1987]. If these structural changes are significant with respect to viscous flow the two
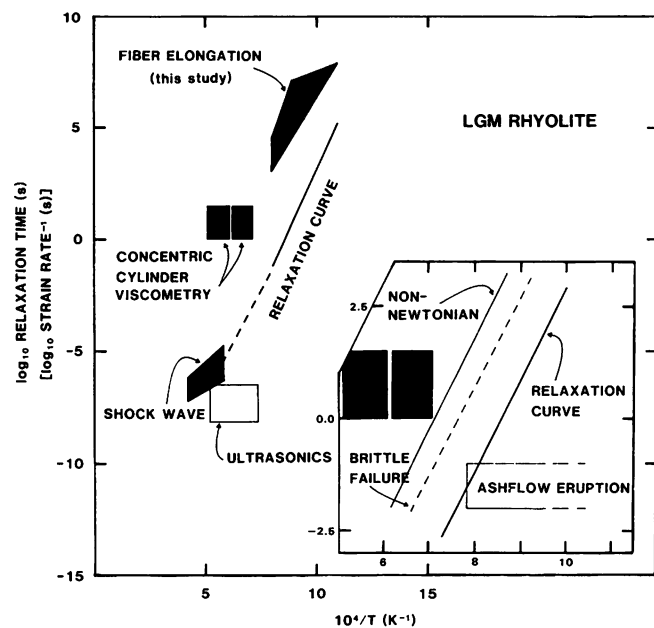
Fig. 6. Locations of various experimental techniques with respect to structural relaxation in Little Glass Mountain rhyolite. The relaxation curve is calculated from the present measurements (solid line) and from the method of *Shaw* [1972] (dashed line). The concentric cylinder viscometry methods are (1) normal torque [*Dingwell*, 1989] and (2) high torque [*Spera et al.*, 1988]. The ultrasonics location is that of *Sato and Manghnani* [1985]. The fiber elongation area is that of the present study. The location of shock wave experiments is estimated using equation 11 of *Dingwell and Webb* [1989], together with the shock wave parameters and high-pressure moduli of *Rigden et al.* [1988] and the relaxation time of the present rhyolite.

types of measurements (low strain, frequency domain and high strain, time domain) may not necessarily result in equivalent nonequilibrium properties being observed in the non-Newtonian region.

Brittle Failure

The ultimate result of loading the melt fibers to the high stresses required to reach non-Newtonian strain rates is brittle failure of the fiber. Such failure is observed to occur without tapering or necking down of the fiber. This observation of brittle failure illustrates that in natural processes, stresses sufficiently high to induce brittle failure are also capable of inducing non-Newtonian flow. This observation would not be possible from investigations of the glass transition made using frequency domain techniques alone.

The inset of Figure 6 illustrates the relationship between the onset of non-Newtonian flow, the brittle failure of the fiber and the τ curve, calculated from the Maxwell relationship. The three phenomena are, to a first approximation, parallel curves in strain rate-temperature space. The non-Newtonian onset occurs three log units of time above the relaxation curve. This is followed, in the case of continued flow at increasing strain rate, by the brittle failure curve, ~ 2 $\log_{10}$ units above the relaxation curve; as observed by *Simmons et al.* [1982]. This generalization of parallel slopes for the three phenomena is based on the composition (nephelinite to rhyolite) and temperature invariance ($818°-674°C$) of the 3 log unit differences between the non-Newtonian onset

and the τ curve. This is equivalent to an assumption of thermorheological simplicity (or the time-temperature equivalence principle). While the assumption of thermorheological simplicity works well over the $100°-200°$ range of many studies, it is, however, possible that more complex behavior would be observed over larger temperature ranges.

Geological Implications

The present study has demonstrated that the stress-strain rate relationships of silicate melts of geological interest (rhyolite, andesite, basalt, and nephelinite) all become nonlinear with increasing strain rate. The strain rates required to induce non-Newtonian behavior correspond to time scales 3 orders of magnitude less than the structural relaxation time scale for the melt. The stresses required for such behavior are of the order of 10^8 Pa and are near the tensile strength of silicate melts. There is no significant temperature or compositional effect observed to date.

Eruptive processes involving rhyolite in this strain rate-temperature range should exhibit such non-Newtonian stress-strain rate behavior. It is clear from the observation of volcanic ash that brittle failure of the rhyolite occurs during ash flow eruptions. This, combined with the results of the present study, leads us to suggest that the viscous flow of silicate melts during eruptions involving brittle failure of the magma will pass through a stage of unrelaxed, non-Newtonian deformation. In this study we have observed up to 2.5 $\log_{10}$ Pa s reduction in viscosity (Figures 3 and 4). Such behavior may also occur during natural deformation processes. We suggest that modeling of the fluid mechanics of magmatic eruptions and of the strain history of rhyolitic glasses include the consideration of non-Newtonian melt viscosity in the appropriate range of strain rates.

The present study illustrates that the occurrence of non-Newtonian viscosity is scaled to the low strain rate, relaxed, Newtonian shear viscosity of the liquid. Although this simplifies the composition dependence of relaxation in silicate melts, it does not remove it. An isothermal comparison of the Newtonian, relaxed viscosities of melts of rhyolite and nephelinite (a difference of ~ 4 $\log_{10}$ Pa s at $1400°C$) reveals how sensitive viscosity is to melt composition. After temperature, the most important factor in determining melt viscosity is water content. Qualitatively, the effect of water is to reduce the relaxed melt viscosity and the corresponding relaxation time of the melt. During ascent of a crystal-poor, water-bearing rhyolite, it is possible that water loss could increase the relaxation time of the melt into the range of the time scale (strain rate^{-1}) of the magma ascent. If the strain rate were maintained, the result would be non-Newtonian flow of the liquid.

The glass transition frequency ($f^{-1} = 2\pi\tau$) also has implications for seismic studies. Taking the onset of non-Newtonian behavior to occur 3 orders of magnitude above the relaxation time; nonlinear stress-strain rate behavior and increasing velocity and attenuation of seismic waves is expected to occur for wave frequencies <10 Hz for melts with shear viscosities $>10^{5.6}$ Pa s (e.g., dry rhyolite at $1050°-1250°C$; rhyolite + 5% H_2O at $575°-725°C$).

4. SUMMARY

The non-Newtonian rheology of four geologic melt compositions (rhyolite, andesite, basalt, and nephelinite) has

been experimentally observed using the fiber elongation technique at high stresses and strain rates. The strain rates at which non-Newtonian behavior occurs can be estimated from the Maxwell relationship. In the present study, melts become significantly non-Newtonian at strain rates corresponding to deformation time scales 3 orders of magnitude slower than the calculated relaxation time. The timescales of Si-O bond exchange, the onset of non-Newtonian flow and the diffusive jump of O anions are related, supporting the proposal that the translation of O anions is the mechanism of viscous flow and the origin of the glass transition.

Non-Newtonian viscous flow precedes brittle failure of silicate melts in these experiments. The same behavior is expected to occur in natural processes, for example, prior to the production of volcanic ash during explosive rhyolitic eruptions. The propagation and attenuation of seismic waves will be strongly frequency dependent in silicate melts whose viscosity is greater than $10^{5.6}$ Pa s.

REFERENCES

Angell C. A., and L. M. Torrell, Short time structural relaxation processes in liquids: Comparison of experimental and computer simulation glass transition of picosecond timescales, *J. Chem. Phys.*, *78*, 937–945, 1983.
Bansal, N. P., and R. H. Doremus, *Handbook of Glass Properties*, Academic, San Diego, Calif., 1986.
Bottinga, Y., and D. F. Weill, The viscosity of magmatic silicate liquids: a model for calculation, *Am. J. Sci.*, *272*, 438–475, 1972.
Brückner, R., Structural aspects of highly deformed melts, *J. Non Cryst. Solids*, *95–96*, 961–968, 1987.
Chayes, F., A world data base for igneous petrology, *Year Book Carnegie Inst. Washington*, *74*, 549–550, 1975.
Christensen, R. M., *Theory of Viscoelasticity*, 364 pp., Academic, San Diego, Calif., 1982.
Dingwell, D. B., Effect of fluorine on the viscosity of diopside liquid, *Am. Mineral.*, *74*, 333–338, 1989.
Dingwell, D. B., and S. L. Webb, Structural relaxation in silicate melts and non-Newtonian melt rheology in geologic processes, *Phys. Chem. Mineral.*, *16*, 508–516, 1989.
Dingwell, D. B., C. M. Scarfe, and D. Cronin, The effect of fluorine on viscosities in the system $Na_2O-Al_2O_3-SiO_2$: Implications for phonolites, trachytes and rhyolites, *Am. Mineral.*, *70*, 80–87, 1985.
Ferry, J. D., *Viscoelastic Properties of Polymers*, 641 pp., John Wiley, New York, 1980.
Harris, P. G., W. Q. Kennedy, and C. M. Scarfe, Volcanism versus plutonism: The effect of chemical composition, *Geol. J. Spec. Issue*, *2*, 187–200, 1970.
Herzfeld, K. F., and T. A. Litovitz, *Absorption and Dispersion of Ultrasonic Waves*, 535 pp., Academic, San Diego, Calif., 1959.

Li, J. H., and D. R. Uhlmann, The flow of glass at high stress levels, I, Non-Newtonian behavior of homogeneous 0.08 $Rb_2O \cdot 0.92$ SiO_2 glasses, *J. Non Cryst. Solids*, *3*, 127–147, 1970.
Liu, S.-B., J. F. Stebbins, E. Schneider, and A. Pines, Diffusive motion in alkali silicate melts: A NMR study at high temperature, *Geochim. Cosmochim. Acta*, *52*, 527–538, 1988.
Mazurin, O. V., Glass relaxation, *J. Non Cryst. Solids*, *87*, 392–407, 1986.
Mills, J. J., Low frequency storage and loss moduli of soda-silica glasses in the transformation range, *J. Non Cryst. Solids*, *14*, 255–268, 1974.
Mysen, B. O., Magmatic silicate melts: Relations between bulk composition, structure and properties, Magmatic Processes: Physicochemical Principles, edited by B. O. Mysen, *Spec. Publ. Geochem. Soc.*, *1*, 375–399, 1987.
Nye, J. F., *Physical Properties of Crystals*, 322 pp., Oxford University Press, New York, 1957.
Rigden, S. M., T. J. Ahrens, and E. M. Stolper, Shock compression of molten silicate: Results for a model basaltic composition, *J. Geophys. Res.*, *93*, 367–382, 1988.
Rivers, M. L., and I. S. E. Carmichael, Ultrasonic studies of silicate melts, *J. Geophys. Res.*, *92*, 9247–9270, 1987.
Ryan, M. P., and J. Y. K. Blevins, The viscosity of synthetic and natural silicate melts and glasses at high temperatures and 1 bar (10^5 pascals) pressure and higher pressures, *U.S. Geol. Surv. Bull.*, *1764*, 563 pp., 1987.
Sato, H., and M. H. Manghnani, Ultrasonic Measurements of V_p and Q_p: Relaxation spectrum of complex modulus on basalt melts, *Phys. Earth Planet. Inter.*, *41*, 18–33, 1985.
Scarfe, C. M., D. J. Cronin, J. T. Wenzel, and D. A. Kaufman, Viscosity-temperature relationships at 1 atm in the system diopside-anorthite, *Am. Mineral.*, *68*, 1083–1088, 1983.
Shaw, H. R., Comments on viscosity, crystal settling, and convection in granitic magmas, *Am. J. Sci.*, *263*, 120–152, 1965.
Shaw, H. R., Viscosities of magmatic silicate liquids: An empirical method of prediction, *Am. J. Sci.*, *272*, 870–893, 1972.
Shimizu, N., and I. Kushiro, Diffusivity of oxygen in jadeite and diopside melts at high pressures, *Geochim. Cosmochim. Acta*, *48*, 1295–1303, 1984.
Simmons, J. H., R. K. Mohr, and C. J. Montrose, Non-Newtonian viscous flow in glass, *J. Appl. Phys.*, *53*, 4075–4080, 1982.
Spera, F. J., D. A. Yuen, and S. J. Kirschvink, Thermal boundary layer convection in silicic magma chambers: Effects of temperature-dependent rheology and implications for thermogravitational chemical fractionation, *J. Geophys. Res.*, *87*, 8755–8767, 1982.
Spera, F. J., A. Borgia, J. Strimple, and M. Feigenson, Rheology of melts and magmatic suspensions, 1, Design and calibration of concentric cylinder viscometer with application to rhyolitic magma, *J. Geophys. Res.*, *93*, 10,273–10,294, 1988.
Stebbins, J. F., Effects of temperature and composition on silicate glass structure and dynamics: ^{29}Si NMR results, *J. Non Cryst. Solids*, *106*, 359–369, 1988.

D. B. Dingwell and S. L. Webb, Bayerisches Geoinstitut, Universität Bayreuth, Postfach 10 12 51, 8580 Bayreuth, West Germany.